



Contents lists available at ScienceDirect

Spectrochimica Acta Part A: Molecular and Biomolecular Spectroscopy

journal homepage: www.elsevier.com/locate/saa

Acid–base properties, FT-IR, FT-Raman spectroscopy and computational study of 1-(pyrid-4-yl)piperazine



Y. Sheena Mary^a, C. Yohannan Panicker^{b,*}, Hema Tresa Varghese^a, Christian Van Alsenoy^c, Markéta Procházková^d, Richard Ševčík^d, Pavel Pazdera^d

^a Department of Physics, Fatima Mata National College, Kollam, Kerala, India

^b Department of Physics, TKM College of Arts and Science, Kollam, Kerala, India

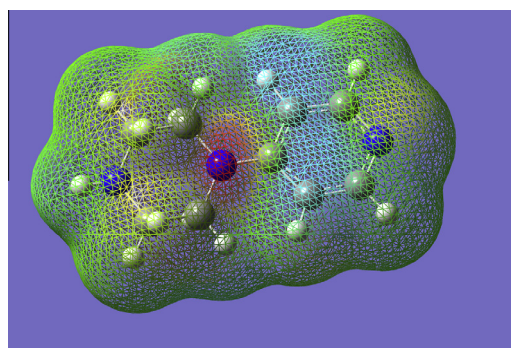
^c Department of Chemistry, University of Antwerp, B2610 Antwerp, Belgium

^d Centre for Syntheses at Sustainable Conditions and Their Management, Faculty of Science, Masaryk University, Brno, Czech Republic

HIGHLIGHTS

- IR, Raman spectra and acid–base properties are reported.
- The wavenumbers are calculated theoretically using Gaussian09 software.
- The geometrical parameters are in agreement with the XRD data.
- Application of FMO, MEP and PED analyses of PyPi.

GRAPHICAL ABSTRACT



ARTICLE INFO

Article history:

Received 31 August 2013

Received in revised form 22 October 2013

Accepted 31 October 2013

Available online 9 November 2013

Keywords:

Piperazine

DFT

PED

FT-IR

FT-Raman

ABSTRACT

We report the vibrational spectral analysis was carried out using FT-IR and FT-Raman spectroscopy for 1-(pyrid-4-yl)piperazine (PyPi). Single crystals of PyPi suitable for X-ray structural analysis were obtained. The acid–base properties are also reported. PyPi supported on a weak acid cation-exchanger in the single protonated form and this system can be used efficiently as the solid supported analogue of 4-N,N-dimethyl-aminopyridine. The complete vibrational assignments of wavenumbers were made on the basis of potential energy distribution. The HOMO and LUMO analysis is used to determine the charge transfer within the molecule and with the molecular electrostatic potential map was applied for the reactivity assessment of PyPi molecule toward proton, electrophiles and nucleophiles as well. The stability of the molecule arising from hyper-conjugative interaction and charge delocalization has been analyzed using NBO analysis. The calculated first hyperpolarizability of PyPi is 17.46 times that of urea.

© 2013 Elsevier B.V. All rights reserved.

Introduction

Piperazine is a potent anthelmintic used in the therapy of ascariasis (roundworms) and oxyuriasis (threadworms/pinworms) infestations. The piperazines were originally named because of

their chemical similarity with piperadine, a constituent of piperine in the black pepper plant. Piperazine owes its anthelmintic activity to its ability to produce flaccid paralysis of the muscles of the parasite [1]. Piperazines have been reported in gene transfer reactions [2] and quaternary piperazinium salts have shown spasmolytic, anthelmintic and germicidal activity. Some piperazine derivatives possess high biological activity for multidrug resistance in cancer and malaria [3]. Gunasekaran and Anita [4] reported the

* Corresponding author. Tel.: +91 9895370968.

E-mail address: cyphyp@rediffmail.com (C.Y. Panicker).

spectral investigation and normal coordinate analysis of piperazine. Panicker et al. reported the spectroscopic investigations of 1-benzylpiperazine [5]. Kesan et al. [6] reported the FT-IR and Raman spectroscopic and quantum chemical investigations of some halide complexes of 1-phenylpiperazine. 1-(Pyrid-4-yl)piperazine (PyPi) belongs to a group 4-N,N-dialkyl analogues of 4-N,N-dimethyl-aminopyridine (DMAP). DMAP and its analogues, for example 4-pyrrolidinopyridine (PPy), are recently useful as catalysts in laboratory and in technological processes, as well. First of all like activators of electrophilic reagents, particularly like activators of acylation reagents in production of chemical and pharmaceutical specialties. DMAP analogues can be used like nucleophilic catalysts for the Morita–Baylis–Hillman reaction. Examples of their using are written in summary publications [7–10]. PyPi is moreover mainly pharmaceutical intermediate in pharmaceutical production. Its structural motive appears in chemical structure of a lot of pharmaceuticals or in chemical structure of potential pharmaceuticals from group of substituted di-sulfonamides. These pharmaceuticals are widely used for softening of pain or for suppressing of pain, which is evoked from bradykinin receptors 1 [11]. Structural motive of PyPi also appears in chemical structure of CXC-chemokine receptor ligands and in chemical structure of 3,4-disubstituted cyclobuten-1,2-diones [12]. These pharmaceuticals are used for treatment for prophylaxis or for treatment for various diseases evoked abnormal production TNF- α and diseases treatable by IL-10 like as acute and chronic inflammatory diseases, allergic and autoimmune diseases [13]. Other type of pharmaceuticals containing structural motive of PyPi are 2,3-dihydro-3-[4-(substituted)piperazinyl]-1H-isindole-1-ones which are used for treatment of hypertension [14], also CCR5 antagonists which are used for treatment of HIV-1 [15], hybrid and isosteric analogues of 1-acetyl-4-dimethylpiperazinium iodide (ADMP) and 1-phenyl-4-dimethylpiperazinium iodide (DMPP). These pharmaceuticals are effective for central nicotinic acetylcholine receptors (nAChRs), which plays main role in neurodegenerative diseases, for example Parkinson and Alzheimer disease [16]. Structural motive of PyPi also appears in μ -opioid receptors (MOR) antagonists [17], in indol compositions for treatment of nephritis [18], in piperazine structural compositions which are used for dissolving of blood clots during heart or brain strokes [19] and in 4-aryl piperazines with positive allosteric modulation of metabotropic glutamate receptors 5 (mGluR5) which are used for treatment of schizophrenic patients [20]. Structural motive of 1-(pyrid-4-yl)piperazine is instead of a lot of its applications in pharmaceutical chemistry main component of ligands which are used in homogeneous catalysis to production of supra-molecular complexes [21]. In the present work, the vibrational spectroscopic studies and acid–base properties of the title compound are reported.

Experimental

Potentiometric titrations were done by using instrument Titroline alpha plus (SCHOTT, Fischer Scientific) and electrode SenTix 21 (WTW). The fraction diagram of all three forms of PyPi in dependence on pH was calculated by using Hydra/Medusa Chemical Equilibrium Database and Plotting Software [22]. X-ray crystal data and structure refinement of PyPi were collected with a KUMA KM-4 kappa four-circle diffractometer. The structure was solved by direct methods using SHELXS86 [23] and refined on F2 for all reflections using SHELXL193 [24]. Single crystals of PyPi suitable for X-ray structural analysis was obtained in the form of white prisms by crystallization from *n*-heptane at room temperature. The PyPi crystallographic data have been deposited with the

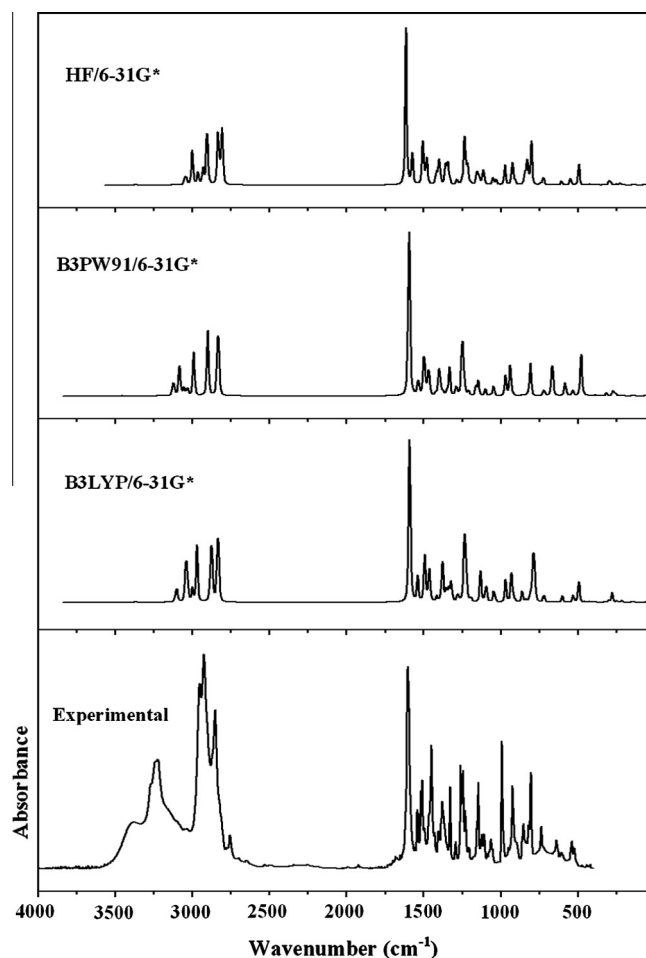


Fig. 1. FT-IR spectrum of 1-(pyrid-4-yl)piperazine.

Cambridge Crystallographic Data Center as supplementary publications number CCDC 836336.

The FT-IR spectrum (Fig. 1) of PyPi was recorded using a Genesis (Unicam Mattson) spectrometer–solid in Nujol. The FT-Raman spectrum (Fig. 2) was obtained on a Bruker, Equinox 55/s spectrometer with FRA Raman socket, 106/s. For an excitation of the spectrum the emission of the Nd:YAG laser was used, excitation wavelength 1064 nm, maximal power 500 mV, measurement on solid sample.

1-(Pyrid-4-yl)piperazine was prepared from 4-(pyridinium-4-yl)piperazin-1-ium dichloride, purchased from Acros Organics (Belgium), by neutralization with 2 equivalent of sodium hydroxide in methanol. Sodium chloride was filtered off, methanol was evaporated and solid white substance was recrystallized from *n*-heptane. M.p. 139.5–140 °C, literature [25] 140 °C (heptane).

¹H NMR spectrum (300 MHz, CDCl₃) δ /ppm: 8.10–8.08 (2H, m, Py-H), 6.52–6.50 (2H, m, Py-H), 3.15–3.12 (4H, m, CH₂), 2.85–2.82 (4H, m, CH₂), 2.69 (NH). Purity controlled by GC was 99.1%.

Acid–base properties

Acid–base constants of 1-(pyrid-4-yl)piperazine were determined by using of potentiometric titrations. Titrations of PyPi (concentration 0.01 M) as a free base form and re-titrations of PyPi in a conjugated bis-protonated form PyPi-2HCl, i.e. 4-(pyridinium-4-yl)piperazin-1-ium dichloride (concentration 0.01 M), were done. Potentiometric titrations of three standards, i.e. piperazine, pyridine and DMAP in a free base form and their re-titrations in

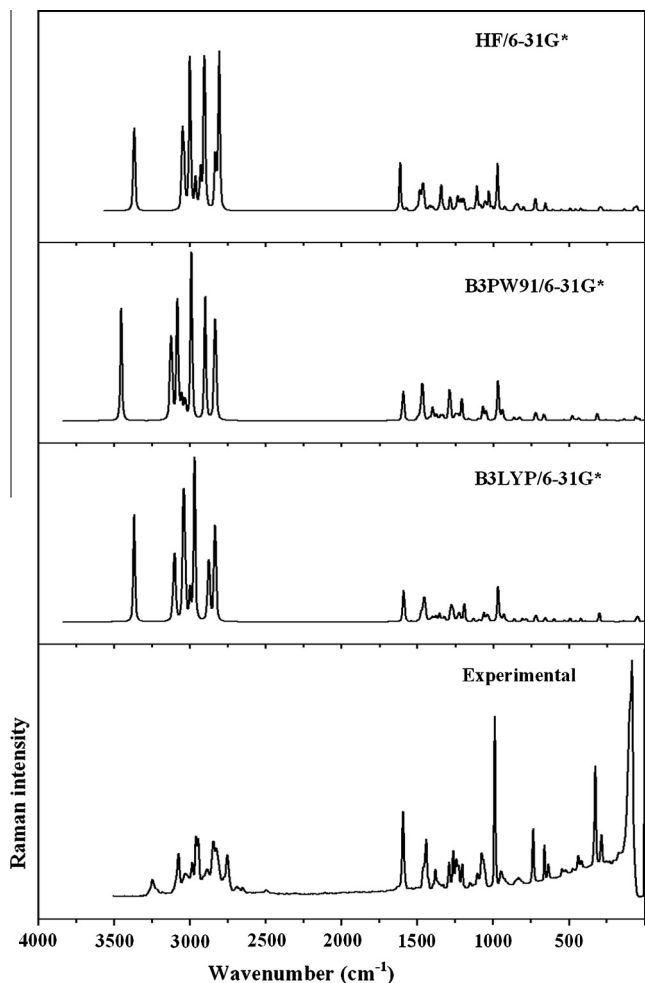


Fig. 2. FT-Raman spectrum of 1-(pyrid-4-yl)piperazine.

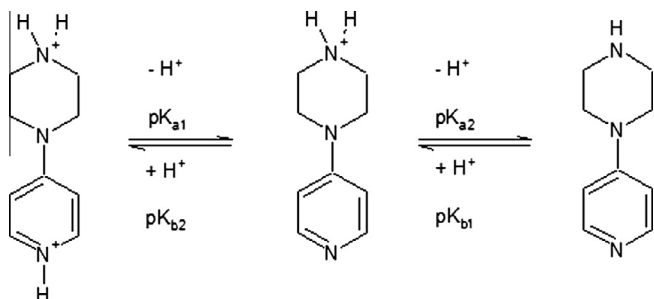


Fig. 3. Scheme of 1-(pyrid-4-yl)piperazine protonation/deprotonation equilibria.

Table 1
Observed pK values of studied amines.

Compound	pKa ₁	pKa ₂	pKb ₂	pKb ₁
1-(Pyrid-4-yl)piperazine	8.99 ± 0.03	7.12 ± 0.04	5.01 ± 0.03	6.88 ± 0.04
Piperazine	9.61 ± 0.04	5.40 ± 0.05	4.39 ± 0.04	8.60 ± 0.05
Pyridine	5.25 ± 0.02	–	–	8.75 ± 0.02
DMAP	8.36 ± 0.03	–	–	5.64 ± 0.03

a conjugated acid form were provided, as well. All potentiometric titrations were realized in aqueous environment under temperature control (295 K) and potentiometric titration were repeated for twelve times. Obtained data were statistically evaluated by software Origin 8.1 and acid–base constants were graphically

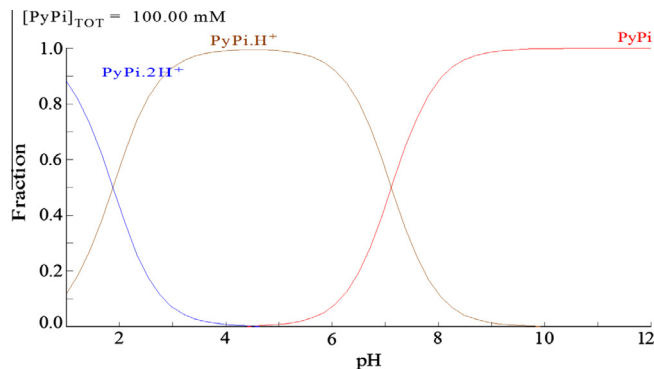


Fig. 4. Fraction diagram.

determined from titration curves after their fitting and differentiating. Scheme of PyPi protonation/deprotonation equilibria is presented in Fig. 3 and obtained results of acid–base constants for PyPi and for all three standards mentioned above are described as pK values in the Table 1. The obtained pKa values of PyPi were used for calculation of fraction diagram (Fig. 4) of PyPi–PyPi·H⁺–PyPi·2H⁺.

Computational details

The vibrational wavenumbers were calculated using the Gaussian09 software package on a personal computer [26]. The computations were performed at HF/6-31G*, B3PW91/6-31G* and B3LYP/6-31G* levels of theory to get the optimized geometry (Fig. 5) and vibrational wavenumbers of the normal modes of the title compound. DFT calculations were carried out with Becke's three-parameter hybrid model using the Lee–Yang–Parr correlation functional (B3LYP) method. Molecular geometries were fully optimized by Berny's optimization algorithm using redundant internal coordinates. Harmonic vibrational wavenumbers were calculated using analytic second derivatives to confirm the convergence to minima in the potential surface. The DFT hybrid B3LYP functional tends also to overestimate the fundamental modes; therefore scaling factors have to be used for obtaining a considerably better agreement with experimental data. Thus, a scaling factor of 0.9613 has been uniformly applied to the B3LYP calculated wavenumbers [27]. The observed disagreement

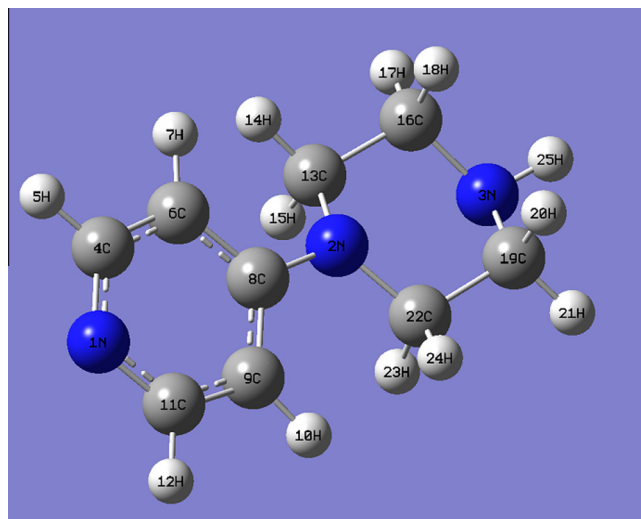


Fig. 5. Optimized geometry (B3LYP) of 1-(pyrid-4-yl)piperazine.

between theory and experiment could be a consequence of the anharmonicity and of the general tendency of the quantum chemical methods to overestimate the force constants at the exact equilibrium geometry. The obtained geometrical parameters are given as supporting information in Table S1. Assignments of the normal modes of vibration are done by Potential Energy Distribution calculation [28] and with the help of Gaussview software [29].

Results and discussion

Acid–base properties

A comparison of the found both pK values of PyPi and pK values for pyridine and piperazine, all given in Table 1, shows that a protonation of neutral 1-(pyrid-4-yl)piperazine molecule starts on the secondary nitrogen N of piperazine part and 4-(pyridin-4-yl)piperazin-1-ium PyPi-H^+ is formed. The tertiary pyridine nitrogen atom in the cation PyPi-H^+ is protonated consequently at lower pH values. Hereinafter, this comparison shows the lower basicity of secondary N_3 in PyPi in the comparison with nitrogen atom of electroneutral piperazine molecule. On the other hand, the basicity of pyridine nitrogen in PyPi-H^+ is higher than the one in separate pyridine molecule, but, nevertheless lower than the basicity of pyridine nitrogen in DMAP. The calculated fraction diagram of the title compound (Fig. 4) displays that just PyPi-H^+ cation is the majority form of PyPi in region pH values between 0 and 7 in water solutions and in protic solvents evidently, too. These findings explain the facts that PyPi can be very effectively supported on weak acid cation-exchanger in the single protonated form and this system can be used efficiently as the solid supported analogue of DMAP for activation of electrophiles in syntheses [30].

IR and Raman spectra

The observed IR, Raman bands and calculated (scaled) wavenumbers and assignments are given in Table 2. The N–H stretching vibrations are generally give rise to bands [31,32] at $3500\text{--}3400\text{ cm}^{-1}$. In the present study, the N–H stretching band is split into a doublet $3383, 3223\text{ cm}^{-1}$ in the IR spectrum owing to Davydov coupling between neighboring units. A similar type of splitting is reported Minitha et al. [33]. The splitting of about 160 cm^{-1} in the IR spectrum is due to strong intermolecular hydrogen bonding. Further more the N–H stretching frequency is red shifted by 144 cm^{-1} in the IR spectrum with a strong intensity from the computed frequency, which indicates the weakening of the N–H bond resulting in proton transfer to the neighboring units [34]. The NH deformation mode δNH is observed at 1428 cm^{-1} in the IR spectrum, 1441 cm^{-1} in the Raman spectrum and at 1443 cm^{-1} theoretically (B3LYP) as expected [35,36]. The out-of-plane NH wag is expected in the region $725 \pm 25\text{ cm}^{-1}$ [36] and in the present case the band at 782 cm^{-1} (B3LYP) is assigned as this mode.

In the vibrations of the CH_2 group, the asymmetric stretching $\nu_{\text{as}}\text{CH}_2$, symmetric stretching $\nu_{\text{s}}\text{CH}_2$, scissoring vibration δCH_2 appears in the regions $3000 \pm 50, 2885 \pm 45$ and $1440 \pm 25\text{ cm}^{-1}$, respectively [35,36]. The B3LYP calculation gives $\nu_{\text{as}}\text{CH}_2$ at $3031, 2999, 2970, 2969\text{ cm}^{-1}$ and $\nu_{\text{s}}\text{CH}_2$ at $2879, 2871, 2835, 2829\text{ cm}^{-1}$. The bands observed at 3034 cm^{-1} in the IR spectrum and at $3028, 2983, 2960, 2886, 2845, 2825\text{ cm}^{-1}$ in the Raman spectrum are assigned as CH_2 stretching modes. The scissoring modes δCH_2 are assigned at $1474, 1463, 1460, 1452\text{ cm}^{-1}$ theoretically and corresponding to this mode, only one band is observed in the IR spectrum at 1449 cm^{-1} . Absorption of hydrocarbons due to CH_2 twisting and wagging vibration [36] is observed in the region $1400\text{--}1150\text{ cm}^{-1}$. These modes are assigned in $1404, 1380, 1292,$

$1230, 1209\text{ cm}^{-1}$ in IR, $1380, 1289, 1228, 1204\text{ cm}^{-1}$ in the Raman spectrum and in the range $1192\text{--}1398\text{ cm}^{-1}$ theoretically. The bands calculated at $1096, 1047, 1044, 837\text{ cm}^{-1}$ were assigned to the rocking modes of CH_2 [36]. The rocking modes are observed at $1107, 1052, 834\text{ cm}^{-1}$ in the IR spectrum and at $1105, 832\text{ cm}^{-1}$ in the Raman spectrum, as expected [36].

For 1-phenylpiperazine, the CH_2 stretching vibrations have been reported at $2944, 2910, 2881$ and 2884 cm^{-1} [37]. Krishnakumar and Seshadri have reported the CH_2 stretching modes of 2-methylpiperazine at 3078 and 2532 cm^{-1} [38]. The CH_2 scissoring vibrations of piperazine molecule were reported at 1455 and 1446 cm^{-1} [39] while these modes are reported at 1452 cm^{-1} for 1-phenylpiperazine [37] and at 1406 and 1293 cm^{-1} for 2-methylpiperazine [38]. The CH_2 scissoring vibrations observed for piperazine and 1-phenylpiperazine are found to be consistent with the results of the title compound. The piperazine ring stretching modes are highly characteristic and in a study on the determination of piperazine rings in ethyleneamines, poly(ethyleneamine) and polyethylenimine by infrared spectroscopy, Spell reported that the piperazine ring was found to be associated with sharp, well define absorptions at $1380\text{--}1345\text{ cm}^{-1}, 1125\text{--}1170\text{ cm}^{-1}$ and $1010\text{--}1025\text{ cm}^{-1}$ regions of IR spectrum [40]. In accordance with Spell [40], we have also observed a very strong peak in the IR spectrum at 1380 cm^{-1} corresponding to CH_2 wagging mode of the piperazine ring. The theoretically calculated corresponding wavenumber for the mode is 1379 cm^{-1} with a PED of 81% and a calculated IR intensity of 70.82. A very sharp and intense band was observed at 1037 cm^{-1} by da Silva et al. [41] and was assigned to the ring CH_2 rocking motions. As stated by Spell, [40] this is one of the most useful bands for detecting the presence of di-substituted piperazines. In the present case, we have also observed a band at 1052 cm^{-1} in the IR spectrum with calculated values 1047 and 1044 cm^{-1} .

For the title compound, the piperazine ring stretching modes are observed at $1146, 1123, 1107, 853\text{ cm}^{-1}$ in the IR spectrum and at $1152, 1105\text{ cm}^{-1}$ in the Raman spectrum. The calculated values corresponding to these modes are $1131, 1130, 1096, 1034, 910$ and 861 cm^{-1} . El-Emam et al. [42] reported the C–N stretching vibrations of the piperazine ring in the region $1154\text{--}756\text{ cm}^{-1}$. The C–C stretching vibrations in the piperazine ring were reported at $972, 903\text{ cm}^{-1}$ [42]. Two absorption characteristic for the piperazine ring at 1130 and 1168 cm^{-1} and assigned for the CN stretching modes were observed by da Silva et al. [41]. In the present case, we have observed bands in the IR spectrum at 1146 and 1123 cm^{-1} corresponding to the piperazine ring stretching modes and the shift in the wavenumber may be attributed to the bulky groups attached to the piperazine ring. Piperazine ring modes are reported at $1240, 1155, 1134, 1043, 1032, 1018, 1002, 974, 880\text{ cm}^{-1}$ theoretically and at $1238, 1143, 1045, 1004, 874\text{ cm}^{-1}$ experimentally [43]. Gunasekaran and Anita reported the piperazine ring stretching modes at $1055, 1173, 1199, 1218, 1268, 1323\text{ cm}^{-1}$ in the IR spectrum and at $1049, 1120, 1186, 1294\text{ cm}^{-1}$ in the Raman spectrum [4].

The infrared spectrum of pyridine looks like that of mono-substituted benzene and the spectrum of substituted pyridines resemble those of substituted benzenes, counting the ring nitrogen as a substituted carbon [36]. Vibrational assignments of the pyridine ring are made by referring to the published studies on selected organic structures [36], Colthup et al. [44], Silverstein et al. [45], Urena et al. [46], Klots [47] and Panicker et al. [48]. The CH stretching vibrations of 4-substituted pyridines are usually observed in the range $3010\text{--}3090\text{ cm}^{-1}$ [47,49,50]. In the present case, the bands observed at 3096 cm^{-1} in the IR spectrum and at 3075 cm^{-1} in the Raman spectrum corresponding CH modes. The B3LYP calculations give these modes at $3109, 3098, 3043$ and 3039 cm^{-1} .

Table 2
Vibrational assignments of 1-(pyrid-4-yl)piperazine.

HF/6-31G*			B3PW91/6-31G*			B3LYP/6-31G*			IR	Raman	Assignments
ν	IR _i	R _A	ν	IR _i	R _A	ν	IR _i	R _A	ν	ν	
3368	0.80	161.78	3453	0.11	199.09	3367	1.19	198.86	3383	3245	ν NH(100)
–	–	–	–	–	–	–	–	–	3223	–	–
3051	9.38	80.11	3127	10.39	122.83	3109	11.24	74.86	–	–	ν CH(97)
3039	17.12	90.39	3120	22.49	88.01	3098	16.98	93.61	3096	3075	ν CH(95)
3002	31.56	104.28	3085	31.62	102.38	3043	28.33	129.37	–	–	ν CH(95)
2998	42.37	120.61	3081	31.07	138.73	3039	41.73	134.01	–	–	ν CH(98)
2962	25.76	45.47	3055	13.97	39.13	3031	19.29	48.89	3034	3028	ν_{as} CH ₂ (94)
2931	33.48	55.44	3033	16.31	39.89	2999	18.83	46.54	–	2983	ν_{as} CH ₂ (96)
2905	56.55	139.65	2991	43.69	164.73	2970	38.45	147.39	–	–	ν_{as} CH ₂ (97)
2903	70.25	109.73	2989	41.72	131.60	2969	47.43	122.39	–	2960	ν_{as} CH ₂ (98)
2834	92.60	63.58	2900	108.33	178.15	2879	82.05	94.49	–	2886	ν_s CH ₂ (91)
2825	33.93	19.96	2898	12.89	23.86	2871	40.63	45.68	–	–	ν_s CH ₂ (90)
2809	86.32	186.82	2835	105.64	191.47	2835	96.85	191.46	–	2845	ν_s CH ₂ (96)
2802	32.55	10.52	2829	46.11	30.28	2829	32.63	11.41	–	2825	ν_s CH ₂ (96)
1614	269.92	38.59	1594	345.72	39.35	1590	267.80	39.26	1603	1594	ν Py(59), δ CH(22)
1574	69.66	2.91	1535	35.53	0.29	1539	37.34	0.80	1536	–	ν Py(66)
1504	105.89	2.91	1497	92.74	4.34	1493	73.26	1.20	1496	–	ν Py(50), δ CH(24)
1486	7.70	12.28	1479	3.03	11.83	1474	3.63	11.32	–	–	δ CH ₂ (85)
1479	4.82	0.82	1471	38.59	9.43	1463	55.52	6.22	–	–	δ CH ₂ (90)
1478	36.79	4.73	1468	0.31	21.53	1460	0.58	7.00	–	–	δ CH ₂ (86)
1466	1.53	17.99	1462	5.03	8.03	1452	0.63	20.10	1449	–	δ CH ₂ (97)
1458	0.47	12.20	1461	12.20	7.70	1443	0.75	6.54	1428	1441	δ NH(61), δ CH ₂ (20)
1423	8.80	3.05	1420	6.45	3.85	1414	8.58	2.66	–	–	δ CH(52), ν Py(22)
1414	17.44	2.58	1400	40.93	12.97	1398	0.33	5.97	1404	–	δ CH ₂ (61), ν Pz(12)
1398	57.36	3.82	1391	13.86	1.56	1379	70.82	6.87	1380	1380	δ CH ₂ (61)
1358	33.69	1.09	1374	8.69	8.40	1355	18.33	9.59	–	–	δ CH ₂ (29), ν C ₈ N ₂ (27)
1345	24.80	14.82	1350	4.88	1.67	1340	16.58	1.50	–	–	δ CH ₂ (74)
1344	15.20	7.33	1346	3.65	4.00	1334	4.73	1.32	1328	1329	δ CH(56), δ CH ₂ (12)
1333	16.99	3.91	1331	50.70	5.55	1320	36.03	6.42	–	–	δ CH ₂ (53), δ CH(17)
1283	10.73	13.52	1290	13.05	28.19	1280	13.25	20.94	1292	1289	δ CH ₂ (71)
1248	7.60	1.91	1285	5.78	13.79	1265	1.33	14.85	1260	1263	ν Py(74)
1233	114.49	14.13	1250	88.88	5.75	1234	129.16	5.85	1245	1243	δ CH ₂ (47), ν C ₈ N ₂ (17)
1215	32.96	7.97	1244	53.98	4.00	1226	20.33	1.28	1230	1228	δ CH ₂ (58), ν Py(14)
1196	5.54	12.85	1232	10.19	6.03	1221	20.32	8.04	–	–	δ CH(68), ν Py(21)
1154	31.69	2.23	1208	7.34	21.60	1192	4.56	17.77	1209	1204	δ CH ₂ (90)
1139	17.81	2.01	1162	15.37	2.02	1131	9.50	1.84	1146	1152	ν Pz(58), δ NH(19)
1115	20.30	2.96	1144	28.23	0.50	1130	36.55	1.54	1123	–	ν Pz(91)
1107	12.74	16.53	1101	6.19	0.47	1096	22.05	2.11	1107	1105	δ CH ₂ (43), ν Pz(42)
1084	0.80	4.22	1098	6.88	1.38	1093	8.81	0.78	1087	1076	δ CH(48), ν Py(20)
1060	0.65	5.02	1068	1.74	13.51	1063	0.16	10.07	1064	1065	δ CH(37), ν Py(33), δ Py(12)
1058	1.05	0.19	1054	1.24	0.77	1047	1.14	0.26	1052	–	δ CH ₂ (74)
1050	11.57	4.51	1048	0.46	6.79	1044	15.51	3.27	–	–	δ CH ₂ (38), δ Pz(30)
1029	9.59	13.76	1045	16.56	3.51	1034	4.75	8.37	–	–	ν Pz(60)
1008	0.26	2.09	974	3.53	4.05	968	33.42	34.56	–	988	ν Py(52), δ Py(20)
974	2.63	1.52	968	35.74	38.50	949	0.16	2.78	949	947	γ CH(92)
972	33.72	31.94	955	0.48	2.09	929	27.60	3.47	–	–	γ CH(51), ν Pz(19)
924	54.06	4.13	937	56.87	10.09	928	22.50	5.01	924	–	γ CH(56), ν Pz(18)
906	6.43	0.11	922	2.07	0.30	910	3.11	0.63	–	–	ν Pz(56), γ CH(22)
855	1.88	3.86	863	1.62	3.73	861	14.81	2.90	853	–	ν Pz(60)
844	9.31	1.41	842	1.04	0.79	837	3.64	0.22	834	832	δ CH ₂ (68)
839	16.99	4.93	826	3.19	4.40	809	10.77	3.81	808	–	γ CH(87)
826	52.00	1.23	807	56.83	0.26	793	40.29	0.41	–	–	γ CH(64), γ C ₈ N ₂ (18), τ Py(14)
801	78.01	2.84	728	0.35	0.10	782	71.32	3.25	–	–	γ NH(45), ν Pz(28)
741	3.76	0.36	720	12.89	10.62	722	3.08	0.50	737	736	τ Py(68), γ CH(14), γ C ₈ N ₂ (13),
723	14.17	9.10	667	24.73	3.81	719	9.45	8.13	–	–	δ Py(27), ν Pz(26), δ C ₈ N ₂ (10)
656	0.65	5.40	664	50.44	4.15	657	0.51	5.24	637	661	δ Py(86)
605	8.55	1.21	582	30.15	0.76	600	9.08	2.86	606	–	δ Py(28), δ Pz(23), δ CH ₂ (12)
548	14.83	1.33	533	11.36	1.23	531	9.28	1.41	539	546	γ C ₈ N ₂ (38), τ Py(38)
494	37.62	1.81	479	87.81	5.32	494	34.89	3.46	472	–	δ Pz(49), δ Py(13), γ NH(11)
456	0.70	1.38	459	1.82	1.34	455	0.91	1.26	442	474	δ Pz(72)
423	2.38	1.88	436	0.94	3.14	423	1.23	2.84	419	417	δ C ₈ N ₂ (66)
399	1.25	0.41	388	0.56	0.38	391	0.30	0.77	–	–	τ Pz(49), τ Py(33)
383	0.15	0.54	382	2.01	0.65	382	0.50	0.14	–	–	τ Py(73)
297	9.77	2.97	314	6.11	6.78	301	2.98	8.04	–	326	τ Pz(32), τ Py(21)
285	4.18	1.78	272	11.99	0.53	277	13.74	0.15	–	286	τ Pz(34), γ C ₈ N ₂ (18), τ Py(17)
248	2.70	0.54	254	4.43	0.87	244	2.54	0.75	–	–	τ Pz(78)
225	5.06	0.61	210	0.59	0.36	215	2.77	0.29	–	–	τ Pz(31), γ C ₈ N ₂ (24), τ Py(13)
135	1.29	1.43	138	1.35	1.70	141	1.58	1.27	–	–	τ Py(33), δ C ₈ N ₂ (24), τ Pz(24)
70	0.34	1.90	59	0.89	4.01	56	0.19	2.78	–	–	γ C ₈ N ₂ (56), τ Pz(10)
54	1.44	3.90	39	0.11	1.85	45	1.41	3.47	–	–	τ CN(54), τ Pz(21)

ν – Stretching; δ – in-plane deformation; γ – out-of-plane deformation; τ – twisting; Pz – piperazine ring; Py – pyridine ring; as – asymmetric; s – symmetric; IR_i – IR intensity; R_A – Raman activity; PED contribution is given in bracket in the assignment column.

For 4-substituted pyridines, the ring stretching vibrations occur in the general region 1600–1280 cm⁻¹ [36,45]. These modes involve stretching and contraction of all the bonds in the ring and interaction between the stretching modes. For the title compound, the pyridine ring stretching modes are assigned at 1603, 1536, 1496, 1260 cm⁻¹ in the IR spectrum and at 1594, 1263 cm⁻¹ in the Raman spectrum. The B3LYP calculations give these modes in the range 1265–1590 cm⁻¹. The ring stretching vibration is active near 1335 ± 35 cm⁻¹ a region which overlaps strongly with that of the CH in-plane deformation and the intensity is in general low [36,51]. Corresponding to this mode, the theoretical value is 1414 cm⁻¹ and no bands are observed experimentally. The pyridine ring breathing mode is expected in the range 1000 ± 10 cm⁻¹ for 4-substituted pyridine [36,46] and in the present case the band observed at 988 cm⁻¹ in the Raman spectrum is assigned as the ring breathing mode.

In mono substituted pyridines, there should be four CH in-plane bending modes and four out-of-plane bending modes and are expected in the regions 1040–1330 and 780–990 cm⁻¹ respectively [36,46]. For the title compound, the CH in-plane modes are observed at 1328, 1087, 1064 cm⁻¹ in the IR spectrum, 1329, 1076, 1065 cm⁻¹ in the Raman spectrum and the out-of-plane CH bending modes at 949, 924, 808 cm⁻¹ in the IR spectrum, 947 cm⁻¹ in the Raman spectrum. The B3LYP calculations give the in-plane and out-of-plane CH modes in the range, 1063–1334 and 793–949 cm⁻¹ as expected [36,46]. The in-plane and out-of-plane ring deformation modes of both rings and other substituent sensitive modes are also identified and assigned (Table 2).

NBO analysis

The natural bond orbitals (NBO) calculations were performed using NBO 3.1 program [52] as implemented in the Gaussian 09 package at the DFT/B3LYP level in order to understand various second-order interactions between the filled orbitals of one subsystem and vacant orbitals of another subsystem, which is a measure of the intermolecular delocalization or hyper-conjugation. NBO analysis provides the most accurate possible 'natural Lewis structure' picture of 'j' because all orbital details are mathematically chosen to include the highest possible percentage of the electron density. A useful aspect of the NBO method is that it gives information about interactions of both filled and virtual orbital spaces that could enhance the analysis of intra and inter molecular interactions.

The second-order Fock-matrix was carried out to evaluate the donor-acceptor interactions in the NBO basis. The interactions result in a loss of occupancy from the localized NBO of the idealized Lewis structure into an empty non-Lewis orbital. For each

donor (*i*) and acceptor (*j*) the stabilization energy (*E*2) associated with the delocalization *i* → *j* is determined as

$$E(2) = \Delta E_{ij} = q_i \frac{(F_{ij})^2}{(E_j - E_i)}$$

q_i is the donor orbital occupancy, *E_i*, *E_j* the diagonal elements, and *F_{ij}* is the off diagonal NBO Fock matrix element.

In NBO analysis large *E*(2) value shows the intensive interaction between electron-donors and electron-acceptors and greater the extent of conjugation of the whole system, the possible intensive interactions are given in Table 3. The second-order perturbation theory analysis of Fock matrix in NBO basis shows intra molecular hyper-conjugative interactions of π-electrons. The intra-molecular hyper-conjugative interactions are formed by the orbital overlap between n(N) and σ*(C–C) bond orbital which results in ICT causing stabilization of the system. The intra-molecular hyper-conjugative interaction of C₉–C₁₁ from of n1(N₁) → σ*(C₉–C₁₁) which increases ED (0.02505e) that weakens the respective bonds leading to stabilization of 9.86 kcal mol⁻¹.

Also another intra-molecular hyper-conjugative interactions are formed by the orbital overlap between n(N₂) and π*(C–C) bond orbital of pyridine part which results in ICT causing stabilization of the system. The strong intra-molecular hyper-conjugative interaction of C₈–C₉ from of n1(N₂) → π*(C₈–C₉) which increases ED (0.40644e) that weakens the respective bonds leading to stabilization of 33.87 kcal mol⁻¹. These interactions are observed as an increase in electron density (ED) in C–C anti bonding orbital that weakens the respective bonds. The increased electron density at the nitrogen atoms leads to the elongation of respective bond length and a lowering of the corresponding stretching wave number. The electron density (ED) is transferred from then(N) to the anti-bonding σ*, π* orbital of the C–C explaining both the elongation and the red shift [53]. The –C–N stretching modes can be used as a good probe for evaluating the bonding configuration around the corresponding atoms and the electronic distribution of the molecule. Hence the above structure is stabilized by these orbital interactions.

The NBO analysis also describes the bonding in terms of the natural hybrid orbital n1(N₂), which occupy a higher energy orbital (–0.25538 a.u.) with considerable p-character (93.99%) and low occupation number (1.76109 a.u) and the other n1(N₁) occupy a lower energy orbital (–0.32149 a.u) with p-character (69.77%) and high occupation number (1.92497 a.u). Thus, a very close to pure p-type lone pair orbital participates in the electron donation to the π*(C–C) orbital for n2(N₂) → π*(C–C) interactions in the compound. The results are tabulated as supporting information in Table S2.

Table 3

Second order perturbation theory analysis of Fock matrix in NBO basis corresponding to the intra-molecular bonds of the title compound.

Donor (<i>i</i>)	Type	ED/e	Acceptor (<i>j</i>)	Type	ED/e (kCal mol ⁻¹)	<i>E</i> (2) ^a (a.u)	<i>E</i> (<i>j</i>)– <i>E</i> (<i>i</i>) ^b (a.u)	<i>F</i> (<i>i,j</i>) ^c
N1–C11	π	1.72616	C4–C6	π*	0.30332	28.57	0.32	0.085
C4–C6	σ	1.98391	N2–C8	σ*	0.03067	4.40	1.16	0.064
C4–C6	π	1.70658	C8–C9	π*	0.40644	22.57	0.28	0.073
C6–C8	σ	1.97368	C8–C9	σ*	0.02335	3.26	1.24	0.057
C8–C9	σ	1.97417	C6–C8	σ*	0.02287	3.36	1.24	0.058
C8–C9	π	1.62621	N1–C11	π*	0.39724	31.49	0.27	0.083
C13–C16	σ	1.98377	N2–C8	σ*	0.03067	4.56	1.16	0.065
C13–C16	σ	1.98408	N2–C8	σ*	0.03067	2.57	1.08	0.047
C19–C22	σ	1.98325	N2–C8	σ*	0.03067	2.68	1.07	0.048
LP (1)N1	n	1.92497	C9–C11	σ*	0.02505	9.86	0.91	0.086
LP (1)N2	n	1.76109	C8–C9	π*	0.40644	33.87	0.29	0.092
LP (1)N3	n	1.92187	C16–H18	σ*	0.03459	7.90	0.72	0.068

^a *E*(2) means energy of hyper-conjugative interactions (stabilization energy in kcal/mol.).

^b Energy difference (a.u.) between donor and acceptor *i* and *j* NBO orbitals.

^c *F*(*i,j*) is the Fock matrix elements (a.u.) between *i* and *j* NBO orbitals.

Geometrical parameters and first hyperpolarizability

For the piperazine ring, El-Emam et al. [42] reported the bond lengths $N_3-C_{16} = 1.465$, $N_3-C_{19} = 1.463$, $C_{19}-C_{22} = 1.514$, $N_2-C_{13} = 1.458$, $N_2-C_{22} = 1.471$, $C_{16}-C_{13} = 1.511$ Å and the corresponding bond lengths of the title compound are 1.461, 1.4605, 1.5297, 1.4696, 1.4638, 1.5275 Å (B3LYP) and 1.4585, 1.4455, 1.5068, 1.4574, 1.4734, 1.5075 Å (XRD), respectively. The B3LYP calculations give the bond angles within the piperazine ring $N_3-C_{19}-C_{22} = 109.7$, $N_3-C_{16}-C_{13} = 109.0$, $N_2-C_{13}-C_{16} = 110.9$, $N_2-C_{22}-C_{19} = 110.6$, $C_{13}-N_2-C_{22} = 112.8^\circ$ and the corresponding XRD values are 110.0° , 109.3° , 107.0° , 112.2° and 114.8° . El-Emam et al. [42] reported the corresponding values as 110.0 , 109.7 , 109.7 , 110.0 and 110.0° for different similar derivatives. Karczmarzyk and Malinka [54] reported the dihedral angles $C_{16}-N_3-C_{19}-C_{22} = 61.1$, $C_{13}-N_2-C_{22}-C_{19} = 60.1$, $N_3-C_{19}-C_{22}-N_2 = -61.5$, $C_{22}-N_2-C_{13}-C_{16} = -58.2$, $C_{19}-N_3-C_{16}-C_{13} = -58.9$, $N_2-C_{13}-C_{16}-N_3 = 57.5^\circ$, which are in agreement with our calculated values, 61.8° , 52.7° , -56.3° , -53.2° , -61.9° and 56.8° . The bond lengths $C_4-N_1 = 1.3415$ (B3LYP), 1.3355 (XRD) and $C_{11}-N_1 = 1.3376$ (B3LYP), 1.3475 (XRD), and $C_8-N_2 = 1.3956$ (B3LYP), 1.3864 Å (XRD) are shorter than the normal C–N single bond length of about 1.48 Å. The shortening of the CN bond lengths reveal the effects of resonance in this part of the molecule [55].

All the carbon–carbon bond lengths in the pyridine ring lie in the range 1.3887–1.4126 (B3LYP), 1.3735–1.4105 Å (XRD) and the CH bond lengths in the range 1.083–1.0898 (B3LYP), 0.949–0.951 Å (XRD). Here for the title compound, the pyridine ring is a regular hexagon with bond length somewhere in between the normal values for a single (1.54 Å) and a double bond (1.33 Å) [56].

The C–N bond lengths of piperazine ring are all close to the average single C–N bond length of 1.48 Å, being $N_2-C_{22} = 1.4638$ (B3LYP), 1.4734 (XRD), $N_2-C_{13} = 1.4696$ (B3LYP), 1.4574 (XRD), $N_3-C_{16} = 1.4610$ (B3LYP), 1.4585 (XRD) and $N_3-C_{19} = 1.4605$ (B3LYP), 1.4455 Å (XRD). The C–N bond lengths in the pyridine ring $C_4-N_1 = 1.3415$ (B3LYP), 1.3355 (XRD), $C_{11}-N_1 = 1.3376$ (B3LYP), 1.3475 Å (XRD) are shorter than the other C–N bonds of the investigated compound. This difference can be attributed to the electronegativity effect of neighbor atoms and groups to these bonds. The resonance effect between C and N atoms and Coulomb repulsive interaction between CH_2 groups give rise to the C–N bond lengths (~ 1.46 Å) to be shorter than the C–C bonds lengths (~ 1.53 Å) in the piperazine ring.

Nonlinear optics deals with the interaction of applied electromagnetic fields in various materials to generate new electromagnetic fields, altered in wavenumber, phase, or other physical properties [57]. Organic molecules able to manipulate photonic signals efficiently are of importance in technologies such as optical communication, optical computing, and dynamic image processing [58,59]. In this context, the dynamic first hyperpolarizability of the title compound is also calculated in the present study. The first hyperpolarizability (β_0) of this novel molecular system is calculated using B3LYP method, based on the finite field approach. In the presence of an applied electric field, the energy of a system is a function of the electric field. First hyperpolarizability is a third rank tensor that can be described by a $3 \times 3 \times 3$ matrix. The 27 components of the 3D matrix can be reduced to 10 components due to the Kleinman symmetry [60]. The components of β are defined as the coefficients in the Taylor series expansion of the energy in the external electric field. When the electric field is weak and homogeneous, this expansion becomes

$$E = E_0 - \sum_i \mu_i F^i - \frac{1}{2} \sum_{ij} \alpha_{ij} F^i F^j - \frac{1}{6} \sum_{ijk} \beta_{ijk} F^i F^j F^k - \frac{1}{24} \sum_{ijkl} \gamma_{ijkl} F^i F^j F^k F^l$$

+ ...

where E_0 is the energy of the unperturbed molecule, F_i is the field at the origin, μ_i , α_{ij} , β_{ijk} and γ_{ijkl} are the components of dipole moment, polarizability, the first hyperpolarizabilities, and second hyperpolarizabilities, respectively. The calculated first hyperpolarizability of the title compound is 2.27×10^{-30} esu, which is comparable with the reported values of similar derivatives [61] and which is 17.46 times that of the standard NLO material urea (0.13×10^{-30} esu) [62]. We conclude that the title compound is an attractive object for future studies of nonlinear optical properties.

Molecular electrostatic potential

Molecular electrostatic potential (MEP) generally present in the space around the molecule by the charge distribution is very useful in understanding the sites of electrophilic attacks and nucleophilic reaction for the study of biological recognition process [63] and hydrogen bonding interactions [64]. In order to predict the molecular reactive sites, the MEP for the title compound is calculated at B3LYP method as shown in Fig. 6. The different values of the electrostatic potential at the surface are represented by different colors. Potential increases in the order red < orange < yellow < green < blue where blue indicates the highest electrostatic potential energy and red indicates the lowest electrostatic potential energy. Intermediary colors represent intermediary electrostatic potentials. As it can be seen from the MEP map of the title compound, the both nitrogen atoms N1 and N3 have the highest value of electrostatic potential energy. This finding is in accordance with the obtained results of acidobasic study of the title compound. On the other hand, the lowest value of electrostatic potential energy on N2 can be explained by conjugation of lone electron pair of N2 with pyridine conjugated π -system. It can be too see from the HOMO plot.

HOMO–LUMO energy gap

The conjugated molecules are characterized by a highest occupied molecular orbital–lowest unoccupied molecular orbital (HOMO–LUMO) separation, which is the result of a significant degree of ICT from the end-capping electron donor to the efficient electron acceptor group through π -conjugated path. The strong charge transfer interaction through π -conjugated bridge results in substantial ground state donor acceptor mixing and the appearance of a charge transfer band in the electronic absorption spectrum. Therefore, an ED transfer occurs from the more aromatic part of the π -conjugated system in the electron donor side to electron withdrawing part. The aromatic orbital components of the molecular orbitals are shown in Fig. 7. The HOMO–LUMO energy

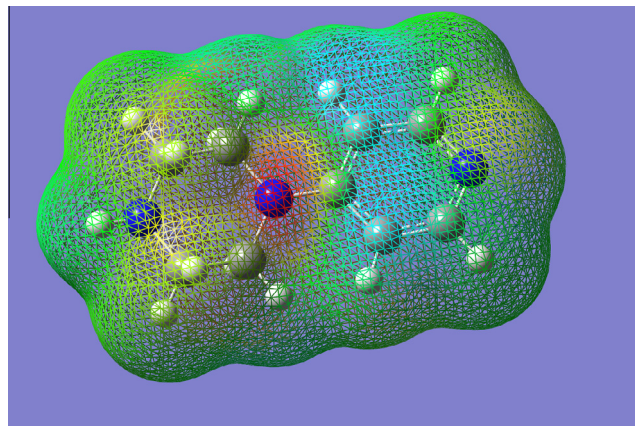


Fig. 6. MEP of 1-(pyrid-4-yl)piperazine.

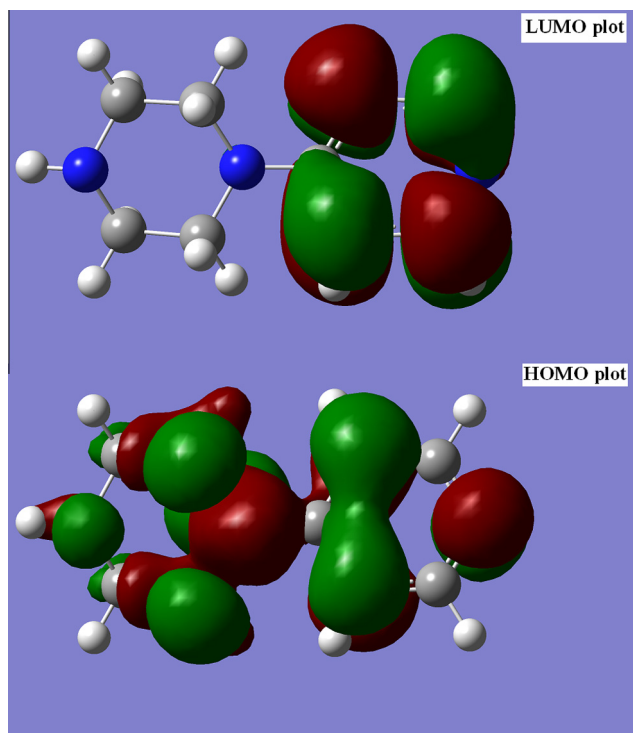


Fig. 7. HOMO and LUMO plots of 1-(pyrid-4-yl)piperazine.

gap values are found at 3.672 eV and HOMO–LUMO energy gap explains the eventual charge transfer interaction takes place within the molecule, which are responsible for the molecular reactivity of the biomedical compound of the title molecule [65]. As it can be seen from the HOMO plot of PyPi, the highest electron population is allocated on N1 of pyridine skeleton. This fact connected with the highest value of electrostatic potential energy, discussed above, shows the kinetic possibility of pyridine nitrogen N1 for binding with electrophiles, e.g. acyl electrophiles, and its ability of an acyl activation. The same HOMO plot demonstrates why the nitrogen N3 is effective for the binding of a proton only, in the case of kinetically controlled interactions, because of its lower electron population. The LUMO plot of PyPi implies the possibility of attack of soft nucleophiles on C4, C6, C9 and C10 respectively, in effect with the same chance.

Conclusion

In this work, the vibrational spectral analysis was carried out using FT-IR and FT-Raman spectroscopy for 1-(pyrid-4-yl)piperazine (PyPi). The computations were performed at HF/6-31G*, B3PW91/6-31G* and B3LYP/6-31G* levels of theory to get the optimized geometry and vibrational wavenumbers of the normal modes of the title compound. The complete vibrational assignments of wavenumbers were made on the basis of potential energy distribution and using Gaussview software. Single crystals of PyPi suitable for X-ray structural analysis was obtained by crystallization from *n*-heptane at room temperature. The acid–base properties are also reported. PyPi can be very effectively supported on weak acid cation-exchanger in the single protonated form and this system can be used efficiently as the solid supported analogue of 4-*N,N*-dimethyl-aminopyridine for activation of electrophiles in syntheses. The HOMO and LUMO analysis is used to determine the charge transfer within the molecule. The stability of the molecule arising from hyper-conjugative interaction and charge delocalization has been analyzed using NBO analysis. The

xcalculated first hyperpolarizability of the title compound is 2.27×10^{-30} esu, which comparable with the reported values of similar derivatives and which is 17.46 times that of the standard NLO material urea (0.13×10^{-30} esu). We conclude that the title compound is an attractive object for future studies of nonlinear optical properties.

Acknowledgement

The authors are thankful to University of Antwerp for access to the university's CalcUA Supercomputer Cluster and Ministry of the Industry and Trade of the Czech Republic for support of Grant No. 2A-1TP/09.

Appendix A. Supplementary material

Supplementary data associated with this article can be found, in the online version, at <http://dx.doi.org/10.1016/j.saa.2013.10.119>.

References

- [1] K. Satoskar, B. Bhandarkar, *Pharmacology and Pharmacotherapeutics*, fifth ed., Bombay Popular Prakashan Pvt. Ltd., Bombay, 1985.
- [2] V. Cecchetti, A. Fravolini, M. Palumbo, C. Sissi, O. Tabarrini, P. Terni, T. Xin, *J. Med. Chem.* 39 (1996) 4952–4957.
- [3] Y. Osa, S. Kobayashi, Y. Sato, Y. Suzuki, K. Takino, T. Takeuchi, Y. Miyata, M. Sakaguchi, H. Takayanagi, *J. Med. Chem.* 46 (2003) 1948–1956.
- [4] S. Gunasekaran, B. Anita, *Indian J. Pure Appl. Phys.* 46 (2008) 833–838.
- [5] C.Y. Panicker, H.T. Varghese, B. Sunil, P.L. Anto, *J. Ultrascientist Phys. Sci.* 24 (2012) 215–224.
- [6] G. Kesan, O. Baglayan, C. Parlak, O. Alver, M. Senyel, *Spectrochim. Acta* 88 (2012) 144–155.
- [7] R. Murugan, E.F.V. Scriven, *Aldrichchim. Acta* 36 (2003) 21–27.
- [8] D.J. Berry, C.V. Digiovanna, S.R. Metrick, R. Murugan, *ARKIVOC* 1 (2001) 201–226.
- [9] Y. Goldberg, *Phase Transfer Catalysis – Selected Problems and Application*, Gordon and Breach Science Publishers, Amsterdam, 1992 (Chapter 7).
- [10] D. Basavaiah, G. Veeraraghavaiah, *Chem. Soc. Rev.* 41 (2012) 68–78.
- [11] M. Reich, S. Schunk, R. Jostock, S. Hees, D.E. Aachen, T. Germann, F.M. Engels, Gruenthal, GmbH, US 2010/0152158 A1.
- [12] A.G. Taveras, J. Cynthia, R.W. Bond, J. Chao, M. Dwyer, M.A. Ferreira, J. Chao, Y. Yu, J.J. Baldwin, B. Kaiser, G. Li, J.R. Merritt, P.J. Bijur, B.H. Nelson Jr., L. Laura, Rokosz Schering Corporation, US 2004/0106794 A1.
- [13] K. Adachi, Y. Aoki, T. Hanano, H. Morimoto, M. Hisadome, Mitsubishi Pharma Corp., US 6455528, 2002.
- [14] C.A. Demerson, I.L. Jirkovský, American Home Products Corp., US 4355031, 1982.
- [15] Y. Liu, E. Zhou, K. Yu, J. Zhu, Y. Zhang, X. Xie, J. Li, H. Jiang, *Molecules* 13 (2008) 2426–2441.
- [16] D. Manetti, A. Bartolini, P.A. Borea, C. Bellucci, S. Dei, C. Ghelardini, F. Gualtieri, M.N. Romanelli, S. Scapecchi, E. Teodori, K. Varani, *Bioorg. Med. Chem.* 7 (1999) 457–465.
- [17] T. Komoto, T. Okada, S. Sato, Y. Niino, T. Oka, T. Sakamoto, *Chem. Pharm. Bull.* 49 (2001) 1314–1320.
- [18] N. Taniguchi, Y. Shirouchi, Nippon Shinyaku Co., WO 01/043746, 2001.
- [19] Y. Hosaka, Y. Miyazaki, T. Matsusue, T. Mukaihira, Mochida Pharmaceutical Co., WO 99/33805, 1999.
- [20] H. Xiong, T.A. Brugel, M. Balestra, D.G. Brown, K.A. Brush, C. Hightower, L. Hinkley, V. Hoesch, J. Kang, G.M. Koether, J.P. McCauley Jr., F.M. McLaren, L.M. Panko, T.R. Simpson, R.W. Smith, J.M. Woods, B. Brockel, V. Chhajlani, R.A. Gadiant, N. Spear, L.A. Sygowski, M. Zhang, J. Arora, N. Breyse, J.M. Wilson, M. Isaac, A. Slassi, M.M. King, *Bioorg. Med. Chem. Lett.* 20 (2010) 7381–7384.
- [21] R. Schneider, M.W. Hosseini, J.M. Planeix, A. De Cian, J. Fischer, *Chem. Commun.* 16 (1998) 1625–1626.
- [22] <http://www.kth.se/che/medusa>.
- [23] G.M. Sheldrick, *Acta Crystallogr., Sect. A* 46 (1990) 467–473.
- [24] G.M. Sheldrick, SHELXL93: Program for Structure Refinement, University of Göttingen, Göttingen, 1993.
- [25] R. Ratouis, J.R. Boissier, C. Dumont, *J. Med. Chem.* 8 (1965) 104–107.
- [26] M.J. Frisch, G.W. Trucks, H.B. Schlegel, G.E. Scuseria, M.A. Robb, J.R. Cheeseman, G. Scalmani, V. Barone, B. Mennucci, G.A. Petersson, H. Nakatsuji, M. Caricato, X. Li, H.P. Hratchian, A.F. Izmaylov, J. Bloino, G. Zheng, J.L. Sonnenberg, M. Hada, M. Ehara, K. Toyota, R. Fukuda, J. Hasegawa, M. Ishida, T. Nakajima, Y. Honda, O. Kitao, H. Nakai, T. Vreven, J.A. Montgomery Jr., J.E. Peralta, F. Ogliaro, M. Bearpark, J.J. Heyd, E. Brothers, K.N. Kudin, V.N. Staroverov, T. Keith, R. Kobayashi, J. Normand, K. Raghavachari, A. Rendell, J.C. Burant, S.S. Iyengar, J. Tomasi, M. Cossi, N. Rega, J.M. Millam, M. Klene, J.E. Knox, J.B. Cross, V. Bakken, C. Adamo, J. Jaramillo, R. Gomperts, R.E. Stratmann, O. Yazyev, A.J. Austin, R. Cammi, C. Pomelli, J.W. Ochterski, R.L. Martin, K. Morokuma, V.G. Zakrzewski,

- G.A. Voth, P. Salvador, J.J. Dannenberg, S. Dapprich, A.D. Daniels, O. Farkas, J.B. Foresman, J.V. Ortiz, J. Cioslowski, D.J. Fox, Gaussian 09, Revision B.01, Gaussian Inc., Wallingford CT, 2010.
- [27] J.B. Foresman, in: E. Frisch (Ed.), *Exploring Chemistry with Electronic Structure Methods: A Guide to Using Gaussian*, Gaussian Inc., Pittsburg, PA, 1996.
- [28] J.M.L. Martin, C. Van Alsenoy, GAR2PED, A Program to Obtain a Potential Energy Distribution from a Gaussian Archive Record, University of Antwerp, Belgium, 2007.
- [29] R. Dennington, T. Keith, J. Millam, Semichem Inc., Shawnee Mission KS, GaussView, Version 5, 2009.
- [30] P. Pazdera, B. Zberovská, M. Procházková, Masaryk University, CZ 303987, 2013.
- [31] A. Spire, M. Barthes, H. Kallouai, G. DeNunzio, *Physics D* 137 (2000) 392–396.
- [32] L.J. Bellami, *The IR Spectra of Complex Molecules*, John Wiley and Sons, New York, 1975.
- [33] R. Minitha, Y.S. Mary, H.T. Varghese, C.Y. Panicker, R. Ravindran, K. Raju, V.M. Nair, *J. Mol. Struct.* 985 (2011) 316–322.
- [34] M. Barthes, G. DeNunzio, G. Ribet, *Synth. Met.* 76 (1996) 337–340.
- [35] G. Socrates, *IR Characteristic Group Frequencies*, John Wiley and Sons, New Yorks, 1981.
- [36] N.P.G. Roeges, *A Guide to the Complete Interpretation of Infrared Spectra of Organic Structures*, Wiley, New York, 1994.
- [37] O. Alver, C. Parlak, M. Senyel, *Spectrochim. Acta* 67A (2007) 793–801.
- [38] V. Krishnakumar, S. Seshadri, *Spectrochim. Acta* 68A (2007) 833–838.
- [39] P.J. Hendra, D.B. Powell, *Spectrochim. Acta* 18 (1962) 299–306.
- [40] H.L. Spell, *Anal. Chem.* 41 (1969) 902–905.
- [41] M.A.S. da Silva, S. deo Pinheiro, T. doss Francisco, F.O.N. da Silva, A.A. Batista, J. Ellena, I.M.M. Carvalho, J.R. de Sousa, F.A. Dias-Filho, E. Longhinotti, I.C.N. Diogenes, *J. Braz. Chem. Soc.* 21 (2010) 1754–1759.
- [42] A.A. El-Emam, Abdul-Malek S. Al-Tamimi, K.A. Al-Rashood, H.N. Misra, V. Narayan, O. Prasad, L. Sinha, *J. Mol. Struct.* 1022 (2012) 49–60.
- [43] I. Sidir, Y.G. Sidir, E. Tasal, C. Ogretir, *J. Mol. Struct.* 980 (2010) 230–244.
- [44] N.B. Colthup, L.H. Daly, S.E. Wiberly, *Introduction to Infrared and Raman spectroscopy*, third ed., Academic Press, Boston, 1990.
- [45] R.M. Silverstein, G.C. Bassler, T.C. Morrill, *Spectrometric Identification of Organic Compounds*, fifth ed., John Wiley and Sons Inc., Singapore, 1991.
- [46] F.P. Urena, M.F. Gomez, J.J.L. Gonzalez, E.M. Torres, *Sepctrochim. Acta* 59A (2003) 2815–2839.
- [47] T.D. Klots, *Spectrochim. Acta* 54A (1998) 1481–1498.
- [48] C.Y. Panicker, H.T. Varaghese, D. Philip, H.I.S. Nogueira, *Spectrochim. Acta* 64A (2006) 744–747.
- [49] V.A. Walters, D.L. Snavely, S.D. Colson, K.B. Wiberg, K.N. Wong, *J. Phys. Chem.* 90 (1986) 592–597.
- [50] J.F. Arenas, J.C. Otero, S.P. Centeno, I.L. Tocon, J. Soto, *Surf. Sci.* 511 (2002) 163–170.
- [51] G. Varsanyi, *Assignments of Vibrational Spectra of Seven Hundred Benzene Derivatives*, Wiley, New York, 1974.
- [52] E.D. Glendening, A.E. Reed, J.E. Carpenter, F. Weinhold, NBO Version 3.1.
- [53] J. Choo, S. Kim, H. Joo, Y. Kwon, *J. Mol. Struct. Theochem.* 587 (2002) 1–8.
- [54] Z. Karczmarzyk, W. Malinka, *X-Ray Struct. Anal. Online* 23 (2007) 151–152.
- [55] S.R. Sheeja, N.A. Mangalam, M.R.P. Kurup, Y.S. Mary, K. Raju, H.T. Varghese, C.Y. Panicker, *J. Mol. Struct.* 973 (2010) 36–46.
- [56] Y.S. Mary, H.T. Varghese, C.Y. Panicker, M. Dolezal, *Spectrochim. Acta* 71A (2008) 725–730.
- [57] Y.R. Shen, *The Principles of Nonlinear Optics*, Wiley, New York, 1984.
- [58] P.V. Kolinsky, *Opt. Eng.* 31 (1992) 11676–11684.
- [59] D.F. Eaton, *Science* 25 (1991) 281–287.
- [60] D.A. Kleinman, *Phys. Rev.* 126 (1962) 1977–1979.
- [61] L.N. Kuleshova, M.Y. Antipin, V.N. Khrustalev, D.V. Gusev, E.S. Bobrikova, *Kristallografiya* 48 (2003) 594–601.
- [62] M. Adant, L. Dupuis, L. Bredas, *Int. J. Quantum Chem.* 56 (2004) 497–507.
- [63] P. Politzer, P.R. Laurence, K. Jayasuriya, *Health Persp.* 61 (1985) 191–202.
- [64] P. Politzer, P. Lane, *Struct. Chem.* 61 (1990) 159–164.
- [65] A. Lakshmi, V. Balachandran, *J. Mol. Struct.* 1033 (2013) 40–50.